CARBON 84 (2015) 103–117

Available at www.sciencedirect.com

ScienceDirect

journal homepage: www.elsevier.com/locate/carbon

# Boron-doped ultrananocrystalline diamond synthesized with an H-rich/Ar-lean gas system

*Hongjun Zeng* [a,*], *Andrew R. Konicek* [b,1], *Nicolaie Moldovan* [a], *Filippo Mangolini* [b], *Tevis Jacobs* [b], *Ian Wylie* [a], *Prabhu U. Arumugam* [a,2], *Shabnam Siddiqui* [a], *Robert W. Carpick* [c], *John A. Carlisle* [a]

[a] *Advanced Diamond Technologies, Inc., Romeoville, IL 60446, United States*
[b] *Department of Materials Science and Engineering, University of Pennsylvania, Philadelphia, PA 19104, United States*
[c] *Department of Mechanical Engineering and Applied Mechanics, University of Pennsylvania, Philadelphia, PA 19104, United States*

ARTICLE INFO

*Article history:*
Received 19 May 2014
Accepted 26 November 2014
Available online 3 December 2014

ABSTRACT

This paper reports the recent development and applications of conductive boron-doped ultrananocrystalline diamond (BD-UNCD). The authors have determined that BD-UNCD can be synthesized with an H-rich gaseous chemistry and a high $CH_4/H_2$ ratio, which is opposite to previously reported methods with Ar-rich or H-rich gas compositions but utilizing very low $CH_4/H_2$ ratios. The BD-UNCD reported here has a resistivity as low as 0.01 ohm cm, with low roughness (<10 nm) and a wide deposition temperature range (450–850 °C). The properties of this BD-UNCD were studied systematically using resistivity characterization, scanning and transmission electron microscopy, Raman spectroscopy, and roughness measurements. Near Edge X-ray Absorption Fine Structure (NEXAFS) spectroscopy confirms that up to 97% of the UNCD is deposited as $sp^3$ carbon. These various measurements also reveal additional special properties for this material, such as an "M" shape Raman signature, line-granular nano-cluster texture and high C—H bond surface content. A hypothesis is provided to explain why this new deposition strategy, with H-rich/Ar-lean gas chemistry and a high $CH_4/H_2$ ratio, is able to produce high $sp^3$-content and/or heavily doped UNCD. In addition, a few emerging applications of BD-UNCD in the field of atomic force microscopy, electrochemistry and biosensing are reviewed here.



## 1. Introduction

Ultrananocrystalline diamond (UNCD) is a very recent member of the diamond material family, and has therefore attracted significant interest over the last two decades [1–3]. While maintaining most of the exceptional physical/chemical properties of conventional diamond materials, UNCD has an extremely low grain size (3–5 nm) and roughness (sub-10 nm) independent of thickness, which drives its popularity as an engineering and functional material, especially in the fields of tribology, biology, and micro/nano-technology [4–5]. In conventional polycrystalline diamond coatings, for either nanocrystalline diamond (NCD) or microcrystalline diamond (MCD), the gas composition usually consists of $CH_4$ or another

* *Corresponding author.*
E-mail address: zeng@thindiamond.com (H. Zeng).
[1] Present address: Corporate Strategic Research, ExxonMobil Research and Engineering, Annandale, NJ, United States.
[2] Present address: Institute for Micromanufacturing, Louisiana Tech University, Ruston, LA 71272, United States.
http://dx.doi.org/10.1016/j.carbon.2014.11.057
0008-6223/

carbon source mixed into a large majority of hydrogen gas in a chemical vapor deposition (CVD) reactor. However, in the prior art, UNCD is only synthesized with an Ar-rich/H-lean gas chemistry. Gruen et al. explained that the role of Ar is primarily to assist in the generation of $C_2$ carbon dimers which act as the principal growth species for UNCD [4], while Rabeau et al. proposed that $C_2$ cannot be the growth species. The latter believes that the only function of Ar is that its heavier neutral and ionic continually bombards the growing surface and maintains uniform smoothness of UNCD [6]. In this report, it is demonstrated that Ar-rich gas mixtures are not the only gas system able to produce UNCD. A gas system with hydrogen completely replacing Ar as the majority gas composition, and a methane/hydrogen ratio significantly higher than that in a conventional CVD polycrystalline diamond recipe, is introduced to enhance the renucleation rate. The gas system is different not only from conventional UNCD deposition which employs Ar, but also from conventional polycrystalline diamond depositions which utilize carbon/hydrogen ratios as low as 0.1–0.3% [7]. The focus here will be this H-rich/Ar-lean gas system, for which high levels of boron doping has been realized in UNCD.

As an emerging P-type material, boron-doped diamond (BDD) combines the advantageous mechanical properties of diamond with a wide band gap [8], and a wide potential window with very low background currents when used as an electrochemical electrode [9]. With a similar bonding structure to natural diamond, BDD shows extremely high chemical, biochemical, and electrochemical stability. These properties enable BDD to be applied broadly, for example in the advanced oxidation of harmful chemicals or pathogens [10], for on-site generation (OSG) for chlorine and mixed-oxidants [11–13], and for high sensitivity biosensing [14–16] especially in harsh environments or *in vivo* testing conditions where extreme chemical and physiological inertness is desirable. However, most of the BDD discussed in the literature is the much rougher (and less physiologically inert) NCD or MCD, with typical surface roughness values in excess of 100 nm [17,44]. The rough as-deposited surfaces of these materials complicates further processing or patterning by high resolution photolithography, as well as bonding, or its integration into more complex structures. Although diamond surfaces inherently possess attractive tribological properties [18–20] and high biocompatibility [21–22], the roughness of NCD and MCD actually diminishes their overall tribological and biological compatibility.

While nitrogen-doped UNCD has been studied previously [23–24], boron-doped UNCD (BD-UNCD) has not been systematically described and characterized in the literature. Swain's group reported the smoothest boron-doped diamond yet reported by adding a boron source (solid state BoronPlus and gas state $B_2H_6$) to a conventional Ar-rich UNCD gas system. They produced BDD with a minimum roughness of 34 nm and a resistivity on the order of 0.1 ohm cm [25]. The present authors began developing boron-doped UNCD in 2009, targeting a super smooth, heavily doped UNCD film as a standard material to enable micro- and nano-technology for MEMS and other devices, and for electrochemical and biosensing applications. Through the use of an Ar-lean gas chemistry, heavily boron-doped UNCD with a resistivity as low as 0.01 ohm cm was developed, with almost as low a surface roughness as un-doped UNCD. Since then, such BD-UNCD has been used to fabricate piezo-resistive microcantilevers [26], conductive atomic force microscopy probes, extremely oxidation-resistant electrodes (anodes) and biosensors. To date, there is no report in the literature describing the properties of BD-UNCD in detail. The film synthesis of BD-UNCD and its special properties distinguished it from the conventional BDD will be addressed here. Its signature properties have been revealed by scanning electron microscopy (SEM), transmission electron microscopy (TEM), Raman spectroscopy, and Near Edge X-ray Absorption Fine Structure (NEXAFS), and Atomic Force Microscopy (AFM) etc. Typical applications of this versatile diamond film will also be discussed. Through this report, we expect to deliver the following information to the readers: (1) a gas strategy with H-rich/Ar-lean and high $CH_4/H_2$ ratio is able to provide a reasonable and effective option to realized BD-UNCD. (2) BD-UNCD has high $sp^3$ purity and interesting properties such as minimum roughness, special cluster shape, Raman and NEXAFS signatures, etc. (3) This new gas strategy may be helpful for us to understand the mechanism of UNCD formation and the role of the gases during the deposition and (4) it can be used in certain important applications where the other types of diamond may not be applied successfully or conveniently.

## 2. Experimental

### 2.1. BD-UNCD synthesis

BD-UNCD as deposited at Advanced Diamond Technologies, Inc. utilizes a tungsten hot-filament chemical vapor deposition (HFCVD) reactor. Diamond film growth starts with substrate seeding using commonly-accepted diamond seeding processes such as surface mechanical abrasion with diamond particles or sonication with slurries containing suspended diamond nanoparticles [27]. A high density of diamond particles (usually $10^9$–$10^{12}$/cm$^2$) on the substrate ensures appropriate seeding density which accelerates the onset of diamond film deposition and provides for a more uniform growth rate and thickness. The reactor setup and seeding processes are similar to those reported previously [28–29]. The major difference here is that an H-rich gas system with a $CH_4/H_2$ ratio as high as 10% employed, which is considerably higher than that of the previously reported polycrystalline diamond with high $sp^3$ purity and the chamber pressure is <15 Torr, lower than what is usually used in conventional NCD and MCD deposition. The substrate temperature can be adjusted across a wide temperature range of 400–850 °C, as monitored by thermocouples with their tips touching the back side of witness Si chips. Deposition rates are in the range of 0.5–3 μm/hour, depending on coating temperature and loading area. The boron doping source is gaseous trimethylborane (TMB, i.e., $B(CH_3)_3$) premixed with very high ratio of hydrogen (>90%). The boron-to-carbon ratio in the gas mixture (abbreviated as B/C gas ratio here) can be adjusted across a wide range from 0 to 12,500 ppm (parts per million). Unless specified otherwise,

the BD-UNCD samples reported here were prepared at a chamber pressure of 5 Torr, a substrate temperature of 750 °C and with a 3000 ppm (0.3%) B/C mole ratio.

### 2.2. *Characterization*

The resistivity of the as-deposited BD-UNCD was measured on 1-μm thick thermally oxidized Si wafers up to 12 inch in diameter (see insert of Fig. 1), with a Four Point Resistivity System (Lucas Labs Pro-4). High resolution SEM and TEM were used to study BD-UNCD grain and surface morphology. The accelerating voltage, aperture size and working distance of the SEM were 10 kV, 10 μm and 10 mm, respectively. Transmission electron microscopy (TEM) was performed on atomic force microscope tips composed of undoped UNCD and BD-UNCD. Multiple probes with nominally identical geometries were fabricated from both materials using the molding technique described in [30], which results in sharp monolithic UNCD tips. The probes were imaged using a JEOL 2010F TEM with a field-emission source, using an accelerating voltage of 200 kV. The back sides of the cantilevers were sputter-coated with 100 nm of aluminum to enhance conductivity and prevent charging. In addition, a small amount of conductive epoxy was applied to ensure electrical connection between the UNCD and the TEM sample mount. Raman spectra were obtained using a spectrometer (Control Development 2DMPP) with an frequency-doubled neodymium-doped yttrium aluminum garnet (Nd:YAG) laser. The laser wavelength and power to a sample is 532 nm and 5 mW, respectively. The acquisition time of each Raman spectrum measurement is 10 s. The NEXAFS measurements were performed at the National Synchrotron Light Source (NSLS) at Brookhaven National Laboratory (BNL, Upton, NY). Two beam lines, U7A and U12A, were both employed for acquiring spectra on as-grown UNCD and BD-UNCD films. The photon source of these beam lines utilizes a bending magnet, and which permits a wide range of spectral energy from 100 to 800 eV. The photon flux was $2\times10^{11}$ photons/s/0.1% bandwidth, with a resolution of $\sim1\times10^{-3}$. All measurements were carried out in partial electron yield (PEY) mode at a photon incidence angle (relative to the sample surface) of 90°. The spectra acquired with the U7A beam line were first normalized to the absorption current measured simultaneously from a gold mesh placed in the beam line upstream from the analysis chamber, and then normalized using the absorption of the post-edge region (at 320 eV). The spectra acquired at U12A were first normalized to the absorption current measured under the same experimental conditions as U7A on a sputter-clean platinum sample, and then normalized based upon the absorption in the post-edge region (at 320 eV). The quantification of the $sp^2$ fraction from NEXAFS spectra was performed following the approach described in [31]. Atomic Force Microscopy (AFM, Veeco Nanoscope IIIa) was employed to measure the roughness of BD-UNCD. AFM tapping mode was used to scan a 5 μm × 5 μm area to extract the root mean square (RMS) roughness.

## 3. Results and discussions

### 3.1. *Electrical properties*

Fig. 1 depicts the relationship between resistivity and the B/C gas ratio. This relationship approaches a reciprocal trend, with a reciprocal constant of ~ 300 ohm cm ppm. As the B/C

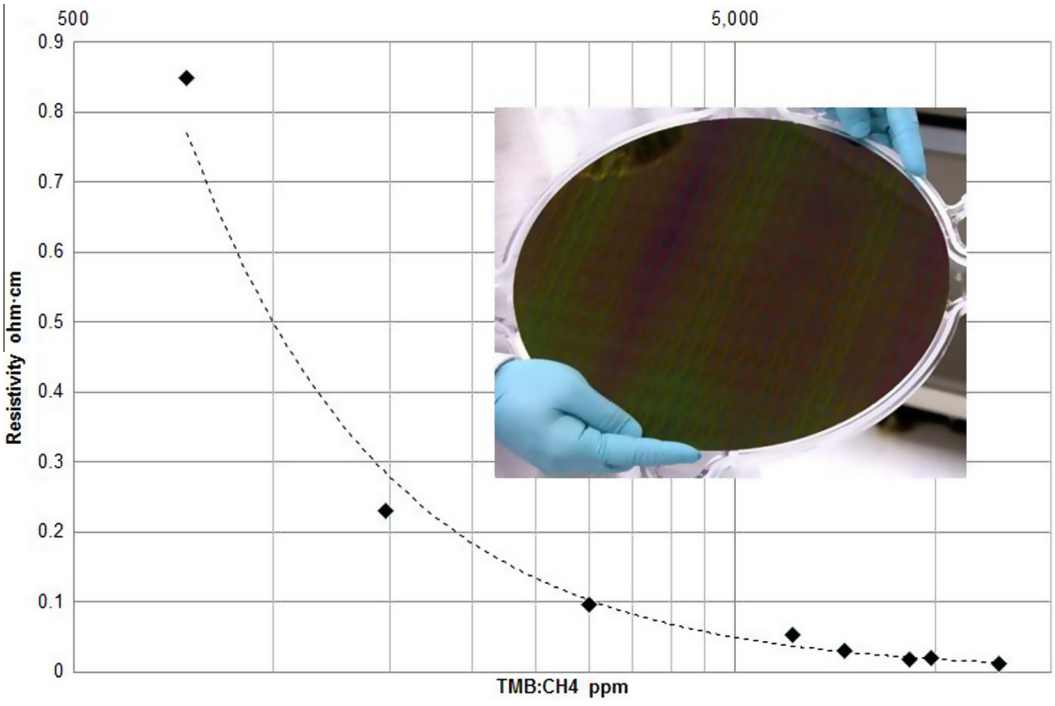


**Fig. 1 – Resistivity vs. B/C gas ratio in gas mixture. Dash line represents a reciprocal curve with a reciprocal constant of 300 ohm cm ppm. Error of all data is <10% except the point at 750 ppm which has an error of 20%. The insert shows a 12-inch BD-UNCD wafer under test. (A color version of this figure can be viewed online.)**

gas ratio is increased in the range from ~9000 to 12,500 ppm, the resistivity tends to saturate at 0.01 ohm cm. When the B/C gas ratio reaches 15,000 ppm or higher, the resistivity increases significantly to about one order of magnitude, to $8 \times 10^{-3}$–$3 \times 10^{-4}$ ohm cm, corresponding to a film structural change from diamond to graphite, which is confirmed by other characterizations below. At the lower doping end of the graph, when the B/C gas ratio decreases to 1000 ppm and less, the resistivity increases to >0.8 ohm cm. Resistivity measurements become more difficult when the B/C gas ratio is decreased further, since the background boron contamination remaining in the reactor from other depositions introduces unaccountable errors in the estimation of the actual boron content in the gas mixture. As a reference, the resistivity of undoped UNCD, produced by a reactor never used for boron doping, was measured at $>10^6$ ohm cm.

Since the authors did not have access to secondary ion mass spectrometry (SIMS) a comparative measurement on the conductivity (the inverse of resistivity) vs. B/C gas ratio was conducted between the data presented here and the data from the literature for boron doped NCD [32]. At a B/C gas ratio of 6660 ppm, the reported conductivity for the heaviest doping is 76 s/cm, while by contrast, the BD-UNCD conductivity measured here was 100 s/cm for the heaviest doping level at 12,500 ppm, which is comparable with the literature value. This conductivity corresponds to a dopant concentration on the order of $10^{21}/cm^3$. Such a heavy doping level could arise from the presence of high boron concentrations at the extremely high internal surface area of UNCD grain boundaries [33]. The carbon atoms at the boundary interfaces and in the boundaries themselves are expected to exhibit more dangling bonds and would therefore be able to retain more boron dopant atoms than inside the grains. A detailed study of the doping at the boundary based on actual SIMS data would be required to substantiate the BD-UNCD doping mechanism.

### 3.2. *Grain and morphology*

Fig. 2a–g depicts BD-UNCD morphologies under high resolution SEM as obtained from different B/C gas ratios. The top view SEM images of heavily doped BD-UNCD (Fig. 2b–f) usually show line-granular structures on the surfaces of the films, rather than the faceted grains of conventional NCDs, which also differ from un-doped UNCD (Fig. 2a) and nitrogen doped UNCD (Fig. 2h). These line-granular structures contain a plurality of grains. The size of the line-granular structures increases as the B/C gas ratio increases until the B/C ratio reaches 9000 ppm. It is hypothesized that such an increase may arise from a slightly increased grain size, similar to that reported from the deposition of nitrogen doped UNCD, when the nitrogen concentration is increased [24]. However, no obvious crystallite facets could be seen under SEM even with a magnification of 100,000×. At B/C ratio above 9000 ppm, the size of the line-granular structure does not increase significantly with increasing the B/C gas ratio. When the B/C gas ratio increases to 12,500 ppm, the film texture starts to change (Fig. 2g), which suggests the onset of graphitization. The typical BD-UNCD line-granular texture shown in Fig. 2b–f is preserved as long as the deposition is conducted at deposition temperatures between 600 and 800 °C. A detailed mechanism for the formation of such special structures is not yet known. When the deposition is conducted at temperatures lower than 600 °C, the facets of crystallites become more evident under SEM as reported in Ref. [34].

It is interesting that the size and shape of these line-granular structures do not significantly change when the thickness is increased from 1 μm (Fig. 2d) to 10 μm (Fig. 2i). The cross sectional SEM images of the BD-UNCD films confirm that the topography of BD-UNCD remains smooth over a thickness range from sub-μm to 10 μm (Fig. 2j and k), which is a feature specific only to UNCD. This is in contrast to MCD whose topography increases dramatically as the film grows (Fig. 2l). It should be noted that BD-UNCD is optically darker than undoped UNCD and NCD, and therefore its thickness is difficult to determine by reflectometry due to low signal strength if the film thickness is more than 1 μm. The thickness is usually measured by cross-sections of witness chips and visualizing the layer under either optical or electron microscopy. Detailed mechanisms for such high optical absorption are unknown, but one explanation is that the concentration of boron at the abrupt grain boundaries increases light absorption. Thickness measurements demonstrate that the deposition rate of BD-UNCD is 5–30% higher than that of un-doped UNCD. Bright-field TEM images, as shown in Fig. 3, enable visualization of individual crystal grains within the BD-UNCD. TEMs on AFM probes fabricated from BD-UNCD, with a B/C ratio of 3000 ppm, show grain diameters ranging from 5 to 15 nm, in accordance with previously published undoped UNCD results [2] or is slightly larger. The diffraction pattern in Fig. 3 consists of continuous and smeared-out circles with smaller dark dots, suggesting randomly oriented small grains of UNCD similar to those reported deposited using Ar-rich gas mixtures [2].

### 3.3. *Raman spectrum*

Fig. 4 shows a comparison of Raman spectra for B/C gas ratios of: 0 (undoped), 750, 1500, 3000, 6000, 9000, and 12,500 ppm respectively. The Raman signal intensity decreases as the B/C gas ratio increases. Therefore, the signals for films obtained with 0–3000 ppm and films with 6000–12,500 ppm B/C gas ratios are represented in separate graphs (Fig. 4a and b, respectively) such that the spectrum details for each ratio are evident. In Fig. 4a, there are four peaks at 1150, 1310–1355, 1470, 1560 $cm^{-1}$, similar to those reported by Swain's Group [25]. However, there are two major differences from that work seen here. The first difference is that there is no sharp peak around 1333 $cm^{-1}$, suggesting a shortage of large size grains and enriched grain boundaries of UNCD [35]. Instead, in this range there is a wide "hybrid" peak combining a weak peak of first order of $sp^3$ (1333 $cm^{-1}$) and a more dominant so-called "D band" peak (1310–1450 $cm^{-1}$) [36]. As the B/C gas ratio increases, the center of the peak shifts from 1355 $cm^{-1}$ (B/C = 0 ppm) to ~1300 $cm^{-1}$ (B/C = 6000 ppm), similar to Ref. [32]. Although the peak shift of the first order of $sp^3$ has been well explained, the shift of the D band peak along with boron concentration has not yet been explained. Such a shift may be caused by content changes at the grain boundary where the number of B—C bonds are increased dramatically. It is known that in UNCD, most of the disordered

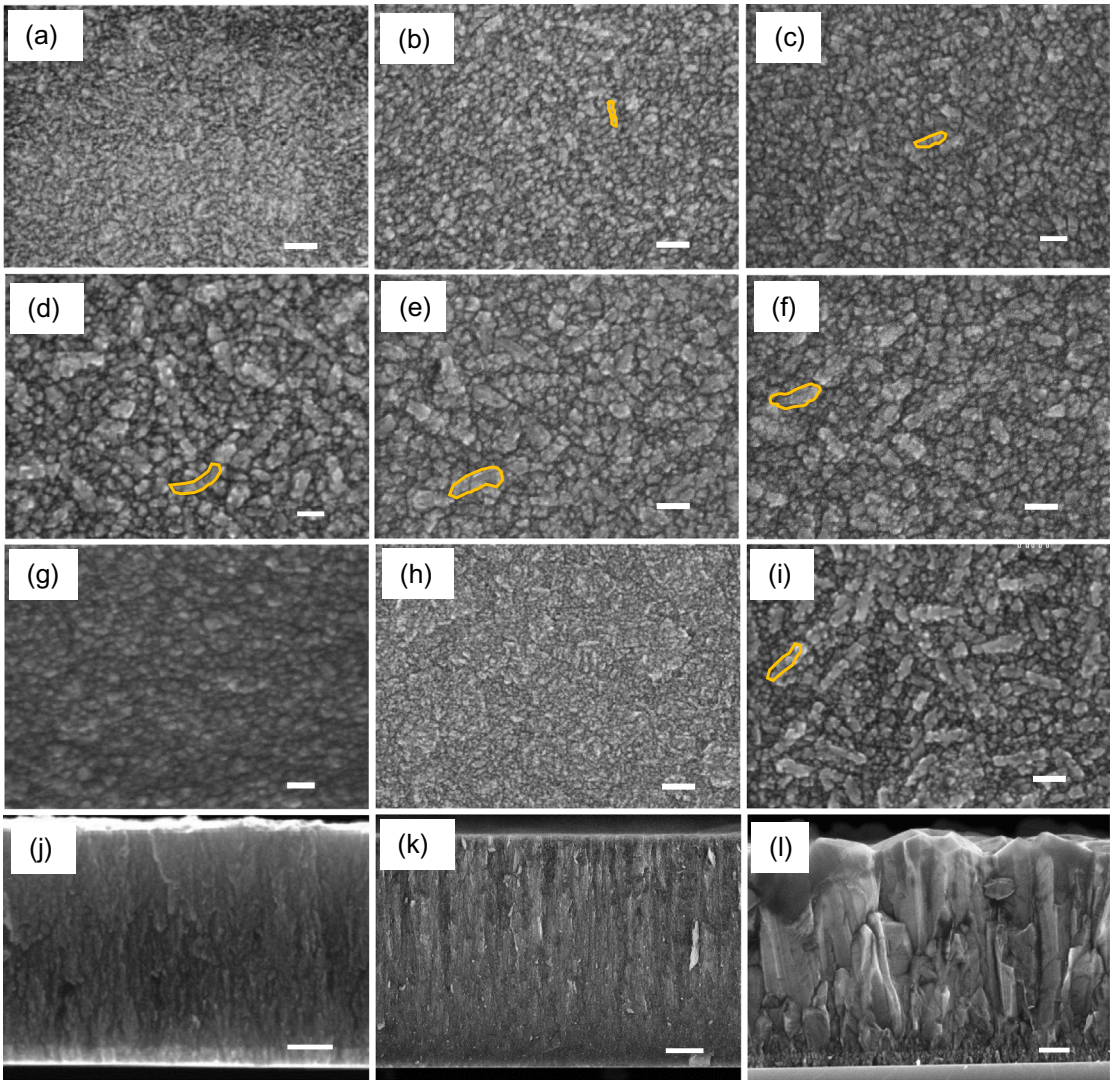


**Fig. 2 – Top-view SEM images of UNCD with B/C gas ratio of (a) 0 ppm i.e., undoped, (b) 750 ppm, (c) 1500 ppm, (d) 3000 ppm, (e) 6000 ppm, (f) 9000 ppm, (g) 12,500 ppm. (h) Top-view image of nitrogen doped UNCD. Film thickness of samples in (a)–(h) is 1 μm. (i) top-view image of BD-UNCD with 10-μm thickness. Cross-section images of BD-UNCD with thickness of (j) 1 μm and (k) 10 μm, and (l) cross-section SEM image of MCD with 1.5-μm thickness. B/C gas ratio of samples from (i) to (l) is 3000 ppm. Orange marks outline the line-granular structures of BD-UNCD. Scale bar in (a)–(i) represents 100 nm, in (j) and (l) represents 200 nm and in (k) represents 2 μm. (A color version of this figure can be viewed online.)**

carbon, represented by the D peak in a Raman spectrum, is confined to the grain boundary, therefore the introduction of excessive boron concentrations at the grain boundary could change the distribution and properties of these disordered carbons.

The second difference in the Raman spectrum from the prior art, are the peaks at 1150 $cm^{-1}$ [37–38] and 1470 $cm^{-1}$ (1450 $cm^{-1}$ as in [38]) according to the work of Show et al. [25]. These peaks are evident only in undoped UNCD or in the low B/C gas ratio H-rich/Ar-lean BD-UNCD of this paper, but become weaker when the B/C gas ratio increases. This was also observed in boron doped NCD and MCD [32], and was explained as a decrease of hydrocarbon content or hydrogen termination. Ferrari's assignment of the 1150 and 1470 $cm^{-1}$ to $\nu_1$ and $\nu_3$ modes of trans-polyacetylene, suggests that the amount of transpolyacetylene decreases as the boron doping level increases. When the B/C gas ratio reaches 3000 ppm, the Raman spectrum of BD-UNCD is dominated by only two major peaks, i.e., the D peak at 1310–1350 $cm^{-1}$ and the G peak at 1560 $cm^{-1}$, featured as an "M" shaped Raman spectrum as shown in Fig. 4c, with a B/C gas ratio of 3000 ppm shown as an example. The "M" shape Raman spectrum was somewhat surprising, since D- and G-peak dominated Raman spectra was usually attributed to a combination of a high percentage of graphite and disordered carbon, but actually, evidence collected from SEM, TEM above and NEXAFS data below, as well as the performances of the BD-UNCD in a multitude of applications, ruled out this suspicion.

At a B/C gas ratio of 6000 ppm, one of the two peaks of the "M" shape spectrum shifts from 1310–1350 to 1220 $cm^{-1}$, as shown in Fig. 4b, while the peak at 1560 $cm^{-1}$ is unaffected.

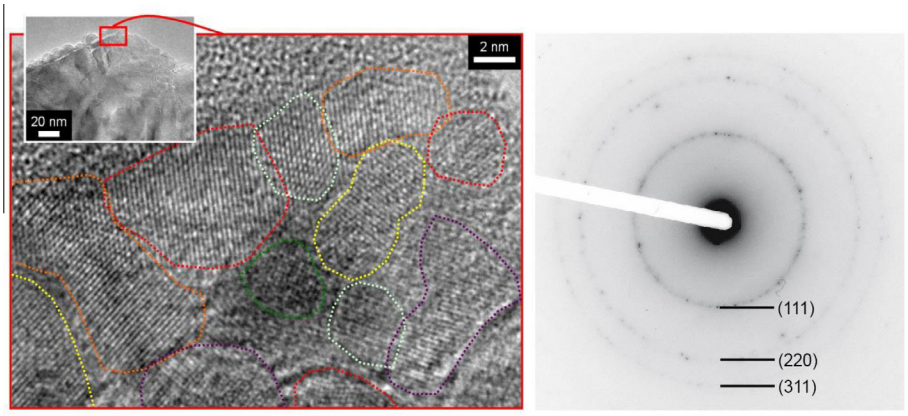


**Fig. 3 – Representative TEM images showing an AFM probe composed of BD-UNCD. Individual grains are readily discernable from lattice fringes and contrast variations. For clarity, colored dashed lines have been superimposed on the image to identify grain boundaries. Because they exhibit a three-dimensional structure, grains can appear to overlap one another. The B/C ratio of the BD-UNCD in the figure is 3000 ppm. The electron diffraction pattern of BD-UNCD is shown on the right. (A color version of this figure can be viewed online.)**

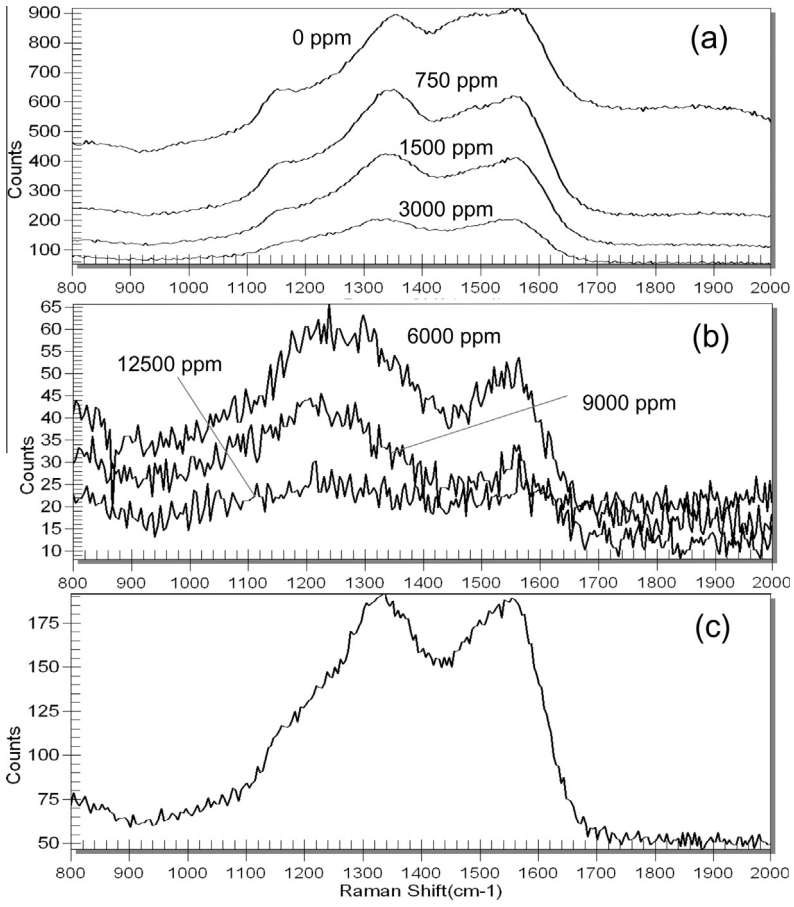


**Fig. 4 – Raman spectra of BD-UNCD with B/C gas ratio of (a) 0–3000 ppm, (b) 6000–12,500 ppm and (c) 3000 ppm-only for best contrast.**

Many authors reported a peak at 1220 $cm^{-1}$ for heavily doped nano- or micro-crystalline diamond Raman spectra, but explanations for this peak are diverse. [32,39–41] As mentioned above, in this study, no obvious facets of crystallites were observed under SEM even with a magnification of 100,000×. It is easy to distinguish the Raman signature of BD-UNCD from that of boron doped MCD, since the Raman spectrum of BD-UNCD has an "M" shape signature, while the Raman spectrum of heavily doped MCD only has one major sharp peak at 1220 $cm^{-1}$, without a G peak from the

grain boundaries, like a "Λ" shape. In Ref. [34], the authors observed that boron does assist in the generation of larger grains, but the presence of boron must be combined with very low deposition temperatures (<500 °C). When the B/C gas ratio is 12,500 ppm or greater, the Raman spectrum acquires a typical graphitization signature, which is compatible with SEM observations.

### 3.4. *Near-Edge X-ray Absorption Fine Structure (NEXAFS) spectroscopy*

NEXAFS is sensitive to oxidation state, hydrogenation, hybridization, and local ordering. It was used to gain insight into the bonding configuration of carbon in BD-UNCD and to compare it with that of undoped UNCD. The carbon 1s NEXAFS spectrum of undoped UNCD, shown in Fig. 5a, exhibits the characteristic features of diamond [42], namely the edge jump at ~289.0 eV, the exciton peak at ~289.3 eV, and the second band gap at ~302.5 eV. All these features are due to the C 1s $\rightarrow \sigma^*$ transition for $sp^3$-hybridized carbon–carbon bonds in the crystalline diamond configuration. Besides the characteristic peaks of diamond, a small absorption band at 285.0 eV was detected. This can be assigned to the C 1s $\rightarrow \pi^*$ transition for disordered $sp^2$-hybridized carbon–carbon bonds. The sources of this $sp^2$-bonded carbon are surface contamination, surface reconstruction, and grain boundaries within the UNCD [42]. The presence of a subtle shoulder at ~287.5 eV can be attributed to the C 1s $\rightarrow \sigma^*$ transition for C—H bonds, indicating hydrogen termination of the UNCD surface [19,43].

The characteristic NEXAFS spectrum of BD-UNCD grown at the same temperature, i.e., 750–800 °C as undoped UNCD, in Fig. 5a exhibits all the characteristic diamond features listed above. Doping UNCD with boron did not affect the fraction of $sp^2$-bonded carbon in the film, but resulted in a subtle change in the absorption of the C 1s $\rightarrow \pi^*$ transition for disordered $sp^2$-hybridized C—C bonds. In contrast, for undoped

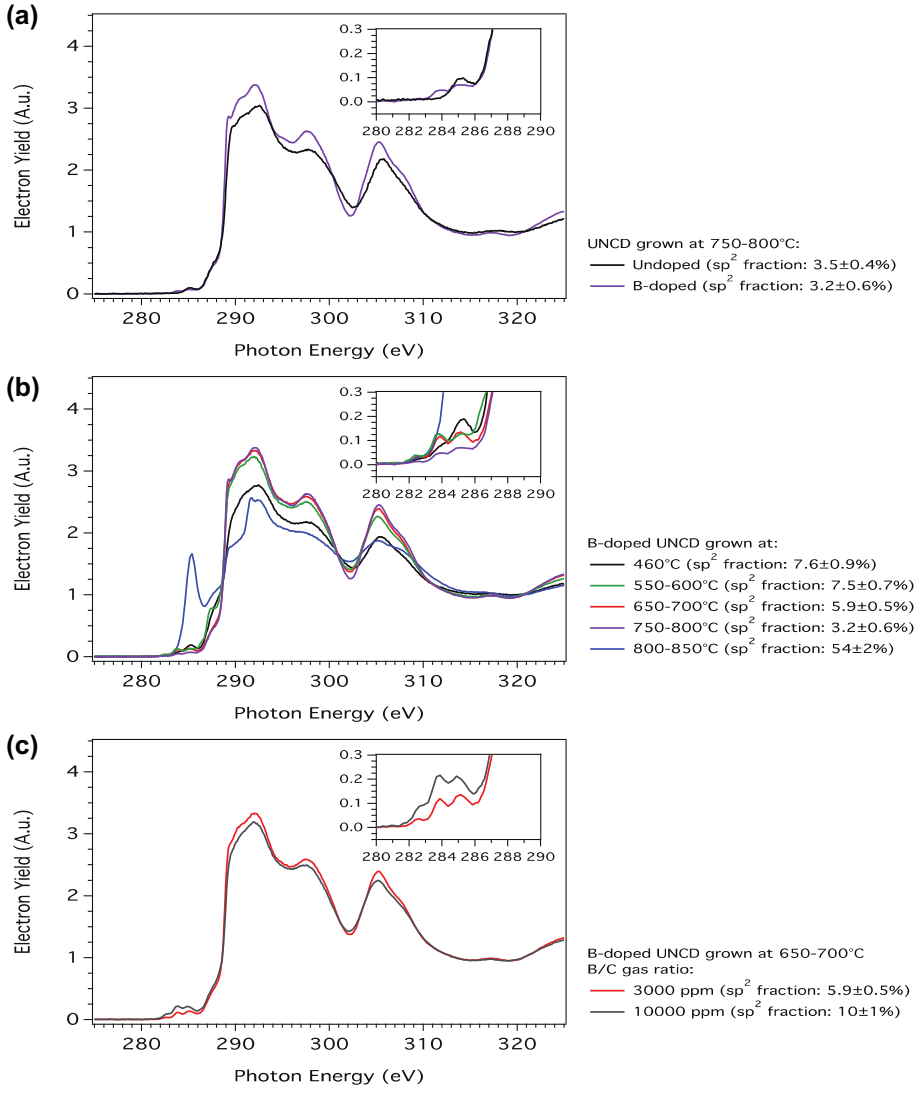


**Fig. 5 – C 1s NEXAFS spectra of: (a) undoped UNCD and BD-UNCD grown at the same temperature (i.e., 750–800 °C); (b) BD-UNCD films grown at different temperatures. B/C gas ratio = 3000 ppm; (c) BD-UNCD films grown at 650–700 °C with different B/C gas ratios. The fraction of $sp^2$-hybridized carbon is reported in the legend. (A color version of this figure can be viewed online.)**

UNCD this feature is symmetric, and upon boron-doping a second band appeared at lower photon energies (~283.8 eV). The detection of this second peak might be attributed to the presence of unoccupied gap states lying below the $\pi^*$ band.

The effect of deposition temperature on the local bonding configuration was also investigated by NEXAFS spectroscopy. The NEXAFS spectra of BD-UNCD, with a constant B/C ratio of 3000 ppm, grown at temperatures ranging from 460 to 850 °C exhibit significant changes (Fig. 5b). In particular, upon increasing the deposition temperature up to 800 °C, the fraction of $sp^2$-bonded carbon was found to slowly decrease down to 3.2%. For deposition temperatures above 800 °C, the fraction of $sp^2$-hybridized carbon in BD-UNCD films significantly increases. The deposition temperature also affected the amount of hydrogen in the near-surface region, i.e., when growing the films at lower temperatures (460–600 °C), the intensity of the shoulder at ~287.5 eV, attributed to the C $1s \rightarrow \sigma^*$ transition for C—H bonds, increases. This indicates that the number of C—H bonds formed at the UNCD surface is higher at lower deposition temperature than that of films deposited at higher temperatures. However, the C—H bond density becomes constant when the deposition temperature is in the range of 650–800 °C. Changing the deposition temperature also resulted in a variation in the absorption of the C $1s \rightarrow \pi^*$ transition for disordered $sp^2$-hybridized C—C bonds. In addition to the band at ~283.8 eV, which was detected in all the spectra of BD-UNCD films independently of the deposition temperature, the NEXAFS spectra of BD-UNCD films grown at temperatures below 750 °C exhibited an additional feature at ~282.3 eV attributable to this C 1s transition.

Fig. 5c shows the impact of different B/C gas ratio on the diamond chemistry. It suggests that the fraction of $sp^2$-bonded carbon in the UNCD film is influenced by the B/C gas ratios: upon increasing this ratio, e.g., from 3000 to 10,000 ppm, which corresponds to increasing by threefold the amount of dopant in the film, the fraction of $sp^2$-bonded carbon only increases slightly. However, the intensity of the shoulder at ~287.5 eV, attributed to the C $1s \rightarrow \sigma^*$ transition for C—H bonds, is not changed by the B/C ratio. Since Fig. 5b demonstrates that the 287.5 eV shoulder does not change with the diamond deposition temperature between 650 and 800 °C, and considering also Fig. 5a and c, one can conclude that the 287.5 eV shoulder is actually unchanged in the whole range of B/C gas ratios, from 0 ppm (undoped) to 10,000 ppm. The BD-UNCD spectrum features 3 peaks at 282.3, 283.8, 285.0 eV, the C $1s \rightarrow \pi^*$ transition for disordered $sp^2$-hybridized carbon–carbon bonds appear in both levels of B/C gas ratios, except the height of these peaks increases with almost the same ratio as the B/C ratio increases.

### 3.5. *Surface roughness*

The dependence of surface roughness vs. film thickness was also studied. This study shows a merely linear dependence, from a very low value of 8 nm RMS at 0.5 μm thickness to 44.5 nm RMS at 13 μm thickness, comparable or slightly smoother than previous work [25]. This demonstrates that the roughness of BD-UNCD increased very slowly as the thickness increases, comparable to that of standard undoped UNCD, suggesting its roughness is much less dependent on thickness than NCD or MCD. As a comparison between BD-UNCD and boron doped NCD, Fig. 6a and b shows AFM images of a 1-μm-thick BD-UNCD and boron doped NCD with 8 nm and 76 nm RMS roughness respectively. For any UNCD, the surface roughness of a diamond film is determined by the renucleation rate and the crystalline growth rate. If the renucleation rate is much higher than the crystalline growth rate, theoretically the diamond would be very smooth. Therefore, if required, by further adjusting the gas ($CH_4$, $H_2$, and TMB) ratios and the reactor pressure to target a faster the renucleation rate, an even smoother BD-UNCD of thick films can be expected. Starting from an already low as-deposited surface

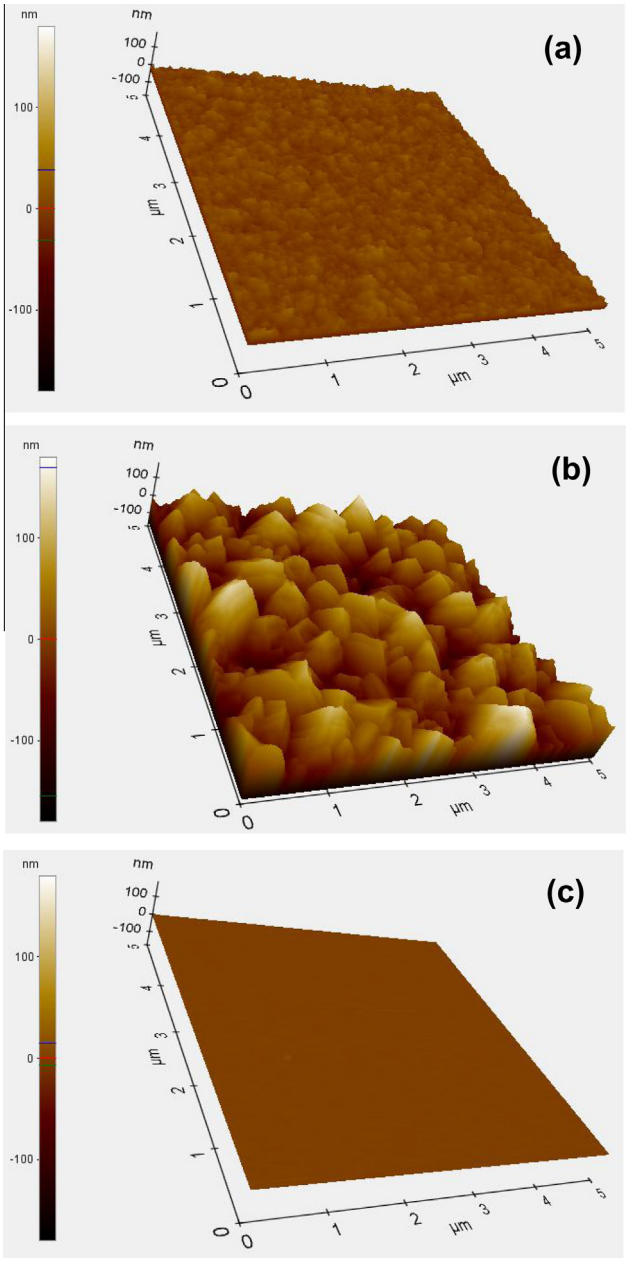


**Fig. 6 – AFM images of (a) BD-UNCD, (b) BDNCD and (c) CMP smoothed BD-UNCD. All images are captured via Tapping Mode with a image capture size of 5 μm × 5 μm². (A color version of this figure can be viewed online.)**

roughness, BD-UNCD can be polished to sub-nanometer roughness much more easily and cheaply than boron doped NCD or MCD. In Fig. 6c, an AFM image is shown of a BD-UNCD surface polished by chemical–mechanical planarization (CMP), with RMS roughness of less than 1 nm. Roughness variations with controlled B/C gas ratios have also been studied. The roughness of films with a standard 1 μm thickness and different B/C gas ratios ranging from 0 to 12,500 ppm were measured and are presented in Table 1. It is interesting that no significant correlation between surface roughness and B/C gas ratio can be observed, while all these films display roughness values typical of UNCD. The size change of the line-granular structures in Fig. 2a–f can even be observed in these SEM images. Therefore, it is possible that the grain size increases when the B/C gas ratio increases. This suggests that the grain size variations caused by boron are too small to contribute significantly to the surface roughness.

### 3.6. *Role of hydrogen*

From the data presented above, it can be deduced that the boron doped diamond films described in this report belongs to the family of UNCD films. They feature very low surface roughness, low correlation between surface roughness and thickness, as well as a non-facet texture under SEM, and very small grain size as determined by TEM. In addition, according to the NEXAFS results, it can be concluded that the $sp^3$ purity of the BD-UNCD is roughly equivalent to that of undoped UNCD reported previously in the literature. More importantly, undoped and doped UNCD can be fabricated with an H-rich gas chemistry instead of an Ar-rich gas chemistry. In a PECVD system, Ar induces the plasma to become very hot, which generates additional precursor species. However, in a HFCVD system, large quantities of precursor species are generated by the high temperature of the filament, so involvement of Ar is unnecessary. The role of Ar in a PECVD reactor for UNCD synthesis is replaced by hot H atoms cracked from $H_2$ gas on the hot filament (at temperatures up to ~2400 °C). The major functions of the hot hydrogen are: (1) reacting with and removing $sp^2$ carbon from the growing diamond film, (2) in a gas system when boron is present, facilitating access to the diamond surface for the boron to react with carbon more efficiently than Ar due to its smaller size and (3) transferring energy to radicals and precursor species $—CH_x$ ($x = 1, 2, 3$), which enhances and accelerates the formation of the UNCD film.

It should be noted that the high $sp^3$ percentage (diamond purity) of BD-UNCD can be realized in a high methane H-rich gas chemistry. This is in contrast to the previous-reported chemistry used for UNCD, NCD and MCD, i.e., the present work shows that high $CH_4/H_2$ ratio is not necessarily connected with low $sp^3$ purity. Conventional NCD or MCD depositions typically use $CH_4/H_2$ gas mixtures, while very low $CH_4/H_2$ ratios are required. To ensure high $sp^3$ purity, a $CH_4$ flow rate of less than 0.5% in NCD/MCD depositions is recommended to prevent the formation of "dirty diamond" [7,25]. For example, even a 1–3% $CH_4/H_2$ ratio would result in up to 50% $sp^2$ impurities [27]. However, the present study demonstrates that UNCD, especially BD-UNCD, can be achieved not only in H-rich/Ar-lean gas system, but also in a gas system with a high concentration of methane (up to 10%), which underscores the fact that a $CH_4/H_2$ ratio is not crucial for diamond quality. The work presented here is guided by a simple hypothesis: that UNCD is a form of diamond with a much more frequent renucleation than NCD or MCD, and therefore any method, such as Ar addition, higher $CH_4/H_2$ ratios or even instant pressure changes, which can maintain a sufficiently high renucleation rate, may all allow the deposition of a UNCD film. Accompanied by the high renucleation rate, formation of a non-diamond carbon phase usually exists, therefor the key to ensure a high quality UNCD deposition is how to efficiently remove the non-diamond carbon "scum" produced during the renucleation process. In the Ar-rich system, $C_2$ may directly lead to diamond lattice construction, with minimum "scum" generation or Ar bombarding may efficiently eliminate the non-diamond "scum". In the H-rich system with high $CH_4/H_2$ gas ratio, the initial nucleation of diamond is slow, a large number of $—CH_x$ species may not contribute to forming diamond, but to forming non-diamond carbon. The non-diamond carbon helps renucleation process for diamond formation, at the same time it deposit on the substrate as "scum", however abundant hot H-atoms are generated to remove the "scum", i.e., react with the excessive non-diamond carbon during the renucleation process, which leads to gaseous products that are easily pumped away.

We use above hypothesis to understand two NCD/UNCD deposition cases. One case is so-called "dirty diamond" [7,25]. As NCD was considered as a thinner version of MCD [44], similar deposition conditions for coating MCD were used to produce NCD, which led to high levels of $sp^2$ impurities when high $CH_4/H_2$ ratios was used. For example, reactor pressures in these depositions were usually set high, typically >30 Torr [45–46], which is more suitable for MCD fabrication but may be a factor causing formation of excessive non-diamond carbon during the deposition of the film. Therefore, a high $sp^2$ content has usually been reported when the concentration of the carbon-based gas was high. Here, the BD-UNCD deposition process employs a high $CH_4/H_2$ ratio, up to 10% and a reactor pressure below 15 Torr, which ensures both a high diamond renucleation rate and a high non-diamond carbon removal rate. With the hypothesis of renucleation and

**Table 1 – Surface roughness vs. B/C gas ratio. Each roughness value is an average from 5 points across a 4 inch BD-UNCD coated wafer.**

| B/C gas ratio (ppm) | 0 | 750 | 1500 | 3000 | 6000 | 9000 | 12,500 |
|---|---|---|---|---|---|---|---|
| RMS (nm) | 6.8 | 6.6 | 6.5 | 7.4 | 6.8 | 7.5 | 6.9 |

"scum" removal for UNCD deposition, the authors understand that under lower pressure, hydrogen may be able to remove more non-diamond components (hydrocarbons and $sp^2$ carbon etc.) to ensure a higher purity of $sp^3$ deposition. Our experiment shows that, while maintaining such a low pressure and decreasing the $CH_4/H_2$ ratio to 0.5–2%, the diamond naturally transitions from UNCD to a NCD form, but with <5% $sp^2$ content measured by NEXAFS (not shown here), much lower than the reported with the similar $CH_4/H_2$ ratio [25,47]. Another case is high graphitization of BD-UNCD at temperature higher than 800 °C, according to the NEXAFS data above regarding $sp^2$ content. With the hypothesis, it can be understood that, when the generation rate of the non-diamond carbon used for renucleation is less than its removing rate by hot hydrogen, the diamond trends to build NCD or MCD; when these two rates are equal, UNCD is generated with the minimum $sp^2$ content confined in grain boundaries; When the generation rate of the non-diamond carbon is higher than removing rate, the $sp^2$ content accumulates too much to be confined by the grain boundaries, and appears in the form of graphite. At the temperature higher than 800 °C, the —$CH_x$ radical's generation rate is higher than what is needed for constructing diamond, therefore the excessive radicals form more non-diamond carbons as temperature reaches or goes higher than this level. These understandings deduced from the hypothesis of renucleation and "scum removal", need to be proved by experiments in the future work. For example, it would be valuable to study the morphology change and $sp^2$ content change along with the pressure variation. From the hypothesis, it can also be expected that, if the $CH_4/H_2$ ratio decreases, which ensures a lower total amount of —$CH_x$, high purity diamond can still be produced at a temperature higher than 800 °C. The related experiments will be conducted and reported as an extended BD-UNCD study.

This report provides an alternative method to fabricate UNCD with an H-rich/Ar-lean gas system. It does not suggest that the H-rich method will entirely replace the conventional Ar-rich method, since the molecular dynamics in the deposition require further study. However, the HFCVD UNCD method provides substantial advantages in large area deposition and reduced capital cost for the reactor. In addition, the H-rich HFCVD approach allows a new overall understanding of the deposition mechanisms for UNCD under these deposition conditions and for those of the Ar-rich PECVD system.

It is also speculated that, by avoiding the use of Ar and its high ionization rate, the possibility of boron–carbon interaction may increase, especially at the grain boundaries. Since the mass of an Ar atom is larger than that of a B atom, in an Ar-rich gas system, the B—C reaction may be hindered by Ar atoms. The kinetic energy of B atoms in the Ar-rich system can be easily changed by collisions with Ar atoms; however, in the H-rich systems, since the mass and volume of an H atom is much smaller than a B atom, H atoms affect the kinetic behavior of B atoms to a lesser degree. For doped UNCD, a popular model is that the grain boundary accommodates the majority of the dopant [33]. In the narrow confines of diamond grain boundaries, H atoms in the Ar-lean HFCVD system, interfere less with boron attachment to carbon's dangling bonds than the larger and more energetic Ar atoms in the Ar-rich PECVD system. Therefore, it is hypothesized that it is easier for an H-rich gas system to realize heavy boron doping and high conductivity UNCD than for an Ar-rich system. This is more significant when low temperature depositions are required, e.g., for semiconductor applications with metallization already present on the wafer. At such low temperatures (~350–450 °C), the concentration of the precursor species near the substrate to be coated is very low and the presence of Ar may be even more "disturbing" both to diamond growth and B—C bond formation given the lower kinetic energy of the species interacting on the surface as compared to higher temperature depositions. In contrast to Ar, when H atoms collide with B atoms, they tend to elastically recoil with the same or similar kinetic energy. Thus, B—C bond formation is not disrupted. In addition, even though H's kinetic energy is low, the chemical reactivity of H atoms is very high with $sp^2$ carbon and therefore hydrocarbons tend to form on the surface of the growing diamond film. Thus the relative efficiency for non-diamond carbon "scum" removal is high for H atoms as compared to Ar, while the interference with boron bond formation with diamond's dangling bonds is low due to the low kinetic energy of H as compared to Ar. Since Ar does not form bonds with carbon, except the limited physical bombarding effect [6], its ability to chemically remove "scum" from the surface of the diamond is minimal or non-existent. The above hypothesis for the mechanism by which H can facilitate BD-UNCD formation is inferred from the known properties of these atoms. However, further detailed research to quantify these mechanisms would be interesting and useful.

## 4. Applications

The BD-UNCD films described above are already being used commercially, with deposition on wafers up to 12 inches in diameter as shown in the inset of Fig. 1. High thickness uniformity (>90%, and as high as >98% across 12" substrates), low roughness and controllable intrinsic stress (both tensile and compressive) enable the application of diamond in MEMS or even NEMS fabrication, with very tight manufacturing tolerances. A series of applications of BD-UNCD have been developed since 2009, including pure monolithic and coated BD-UNCD probes for scanning probe microscopy, electrodes for direct water purification with diamond-generated hydroxyl radicals in aqueous solution and oxidant synthesis, e.g., chlorine/hypochlorite, ozone and peroxodisulphate and other reactive oxidants, and biosensors for pathogen detection and electrochemical analysis.

### 4.1. *Robust, wear-resistant conductive AFM probes*

Conductive BD-UNCD AFM probes exploit two important properties of the material: its low wear rate (due to its hardness and reduced coefficient of friction), and its electrochemical properties (low reactivity and wide electrochemical potential window). We have developed both "all-diamond" probes and diamond coated probes, i.e., the structural material of the probes is silicon but it is subsequently coated with a thin layer of BD-UNCD.

The "all-diamond" probes shown in Fig. 7a, with tips and cantilevers all made from BD-UNCD using a molding technique, involves forming the tip by depositing the diamond onto Si wafers with V-groove pits etched into them, then dissolving the Si [48–49]. Since the grain size for BD-UNCD is smaller than other types of boron doped diamond, BD-UNCD is able to fill the tip molds very accurately and continuously, and the curvature of the released cantilevers of the probes can be close to zero due to precise stress control during the BD-UNCD deposition. The resulting probes' typical tip radii can be as small as 20–50 nm (Fig. 7b). A cross-comparison of the wear properties of different AFM probes, including doped and undoped UNCD probes showed no significant differences between the investigated diamond probes [30]. Additional sharpening to achieve tip radii below 10 nm and aspect-ratio improvements have been demonstrated by oxidation-sharpening the Si molding pits (Fig. 7c) or by additional focused ion beam machining of spikes on the tips, which is able to reach a tip radii below 5 nm (Fig. 7d). The value of hardness in BD-UNCD AFM probes is particularly useful in techniques such as scanning spreading resistance microscopy (SSRM) where the conductive tips need to break through native oxides on conductive surfaces, to achieve electrical contact with the samples. Special tip shapes have been developed for such applications, based on molding in V-grooves etched in Si (3 1 1) wafers [30]. The electrochemical properties of BD-UNCD are of particular value in probes for scanning electrochemical microscopy (SECM), for which special probes have been developed, with complete electrical $SiO_2$ insulation except for a small region of the tip apex.

BD-UNCD can also be used to coat commercial silicon or silicon nitride probes, to confer on them some of the low-wear and conductive properties of the diamond material. Since coating a tip with a film generally increases the tip radius by the thickness of the film, super thin continuous BD-UNCD films were developed for this application. Such probes are of significantly lower cost and have wider design flexibility than "All-diamond" probes, allowing the transformation of any shape of Si or SiN probes into a diamond probe by coating. Because of the extremely small grain size of BD-UNCD, the batch fabrication process produces BD-UNCD probes with diameters as small as 30 nm, with average diameters 70 nm across the entire wafer (Fig. 7e). It is noted that, if a NCD film is coated on an AFM probe, even though the initial grain size is as small as 10–20 nm, its facets would tend to form multiple "spikes" on the top of the probes, leading to a "multi-tip effect" [50]. Another particular phenomena is that the NCD grain size increases much faster on apex locations than on flat or blunted structures, while BD-UNCD maintains almost the same grain size on different textures. Coated AFM probes have been characterized showing tip diameters down to ~20 nm by using a specific tip shape reconstruction method [51]. Wear tests were performed on hard surfaces including quartz, silicon carbide, or UNCD. In one extreme case, the coated probes were scanned for >1 m at a scan speed of 25 μm $s^{-1}$ at temperatures in a range between 25 and 400 °C

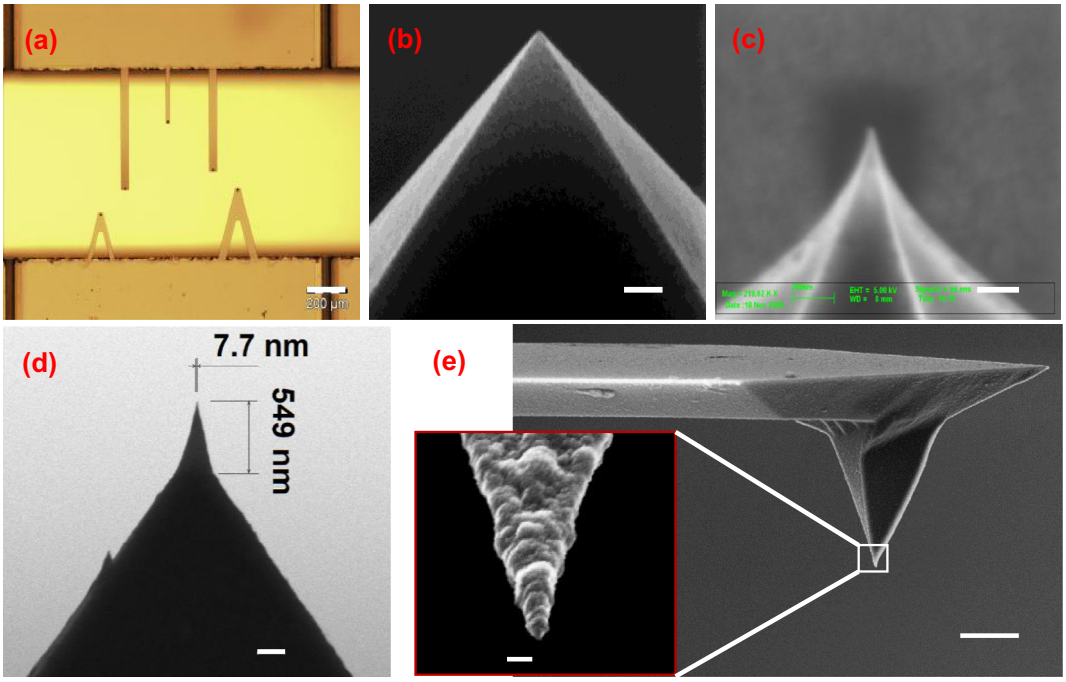


**Fig. 7 – (a) optical micrograph showing monolithic BD-UNCD AFM probes with different cantilever designs, (b) regular unsharpened BD-UNCD AFM probes obtained by direct molding into a Si V-groove, (c) BD-UNCD AFM probes obtained by molding into an oxidation-sharpened Si V-groove, (d) BD-UNCD AFM probe tip with FIB-machined spike and (e) BD-UNCD coated Si AFM probe with the tip magnified in insert. The scale bar in (a) represents 200 μm, in (b)–(c) it represents 100 nm, in (d) it represents 200 nm, in (e) it represents 5 μm and for the insert of (e) it represents 100 nm. (A color version of this figure can be viewed online.)**

under loads of up to 200 nN. Under these conditions, silicon tips are mostly or completely destroyed, while the UNCD tips exhibit much less or no wear [52]. Another case study of the AFM image evolution of the coated probes involved scanning on a rough MCD diamond surface using contact mode. After >200 scans of a 5 μm × 5 μm surface, no change in image quality was observed. By contrast, when Si or SiN probes were tested with the same conditions, the image quality degraded quickly from one scan to the next. BD-UNCD coated Si probes can also be used for low-cost SSRM. If a Si probe is coated with a thick BD-UNCD, a sharp diamond spike can also be shaped on the tip by the aforementioned focused ion beam machining method, saving cost by avoiding an "all-diamond" probe manufacturing process.

### 4.2. *Electrochemically durable electrodes*

BD-UNCD has been proven to be a durable high-current density electrode material. Compared with their MCD counterparts, BD-UNCD's faster deposition rate provides a decreased cost for these expensive industrial electrodes such as those used for water treatment. Like other types of diamond, it has been proven that the integration of BD-UNCD on Nb, Si, Ta, and W is exceptionally robust [53] due to the strength of the chemical bonds between these substrates and their carbides, the stability of their carbides and the relatively low difference in thermal expansion coefficients. In addition, it was observed that film stress for BD-UNCD can be adjusted and its nanometer size grain can conformably fill the micro- or nano-scale structures of a substrate, which significantly reduces film delamination rates and coating defects such as pin-holes [22], therefore the underlying structural materials (metals or silicon) can be protected from electrochemical attack, and the electrodes lifetime is dramatically increased particularly under high current density (anodic oxidation) conditions.

The authors have developed BD-UNCD based electrodes for use within electrochemical cells and systems, as shown in Fig. 8a, with extremely strong adhesion and electrochemical stability even at extreme voltages/current densities in aqueous solutions. A few different types of accelerated lifetime tests for these electrodes have been conducted on these new electrodes. In the most aggressive electrochemical advanced oxidation process (EAOP) protocol, the electrodes were tested up to 4000 A-hr/cm$^2$ in 1 M $NaClO_4$ (i.e., more than 1200 h under test), with a current density of 2500 mA/cm$^2$ applied in galvanostatic mode (i.e., 25 A for a 10 cm$^2$ active area electrode). The end of life of the electrodes was determined by both delamination of the anode material from its substrate and an increase in the cell voltage by more than 3 V. In contrast, commercial Dimensionally Stable Anodes (DSA) or graphite electrodes would only survive a few hours (at best) under such conditions as they are typically operated for commercial chlorine (hypochlorite) production at a current density of 100–150 mA/cm$^2$ or less. In another harsh protocol for the of On-Site Generation (OSG) of oxidants, the electrodes have been tested for more than 4000 A-hr/cm$^2$ in 1 M solar salt (impure NaCl) with an applied current density of 2500 mA/cm$^2$ in galvanostatic mode and more than 16,000 h in 2 M solar salt with an applied current density of 450 mA/cm$^2$ without failure or any observed performance degradation. The BD-UNCD coated electrodes are now being applied widely for the OSG of ozone, chlorine (hypochlorite) (Fig. 8b and c), peroxodisulfate, and peroxodicarbonate, EAOP of wastewater, and direct wastewater treatment via the production of hydroxyl radicals on the diamond surface.

### 4.3. *Reliable and highly versatile sensors*

Advanced microsensors that can reliably detect target analytes in minimally prepared complex samples in real-time represent a formidable challenge for remote environmental monitoring, point-of-use diagnostics, personalized medicine and national security. The two principle issues for the development of integrated electrochemical microsensor are the achievement of highly stable active bio interfaces that interact with and measure analytes of interest, and the engineering of highly robust transducer electrode materials. This second issue is even more challenging when the sensor also fulfills the desired objectives of being ultra-small in size, versatile in immobilizing a wide range of bio layers, uses simple chemistries in functionalizing biomolecules, promotes long-term functional stability of bio layers, and is amenable to scale-up and large volume manufacturing. BD-UNCD is one of the most promising electrode materials because of its superior electrochemical properties as compared to noble metals and sp$^2$ hybridized carbon materials [54]. The electrochemical properties of diamond electrodes were found to be

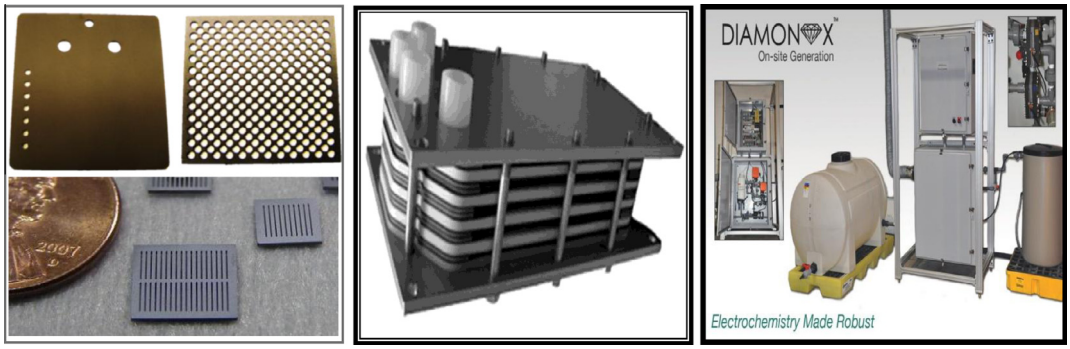


**Fig. 8 – (a) BD-UNCD electrodes with different geometries and substrates, (b) an OSG cell with BD-UNCD electrodes and (c) an OSG system with BD-UNCD electrodes. (A color version of this figure can be viewed online.)**

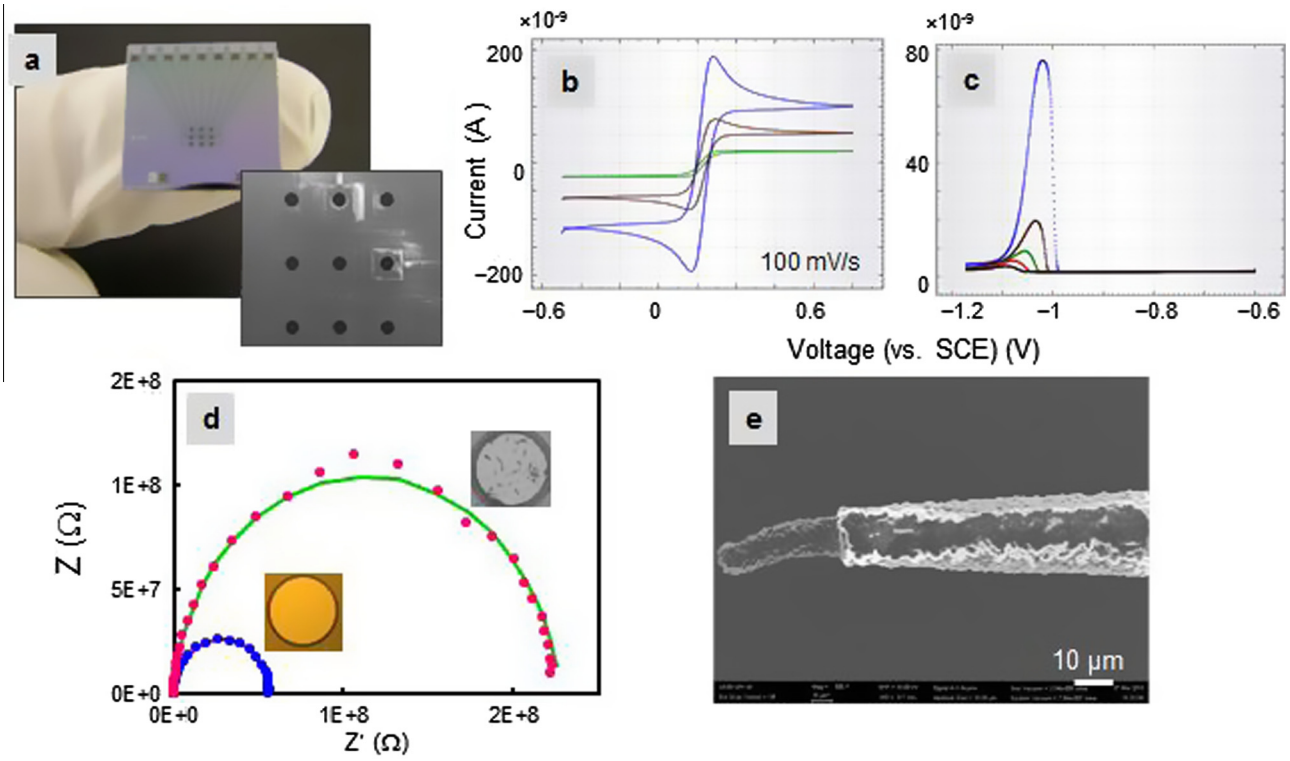


**Fig. 9 – Biological and chemical sensing applications of UNCD 3 × 3 microarrays. (a) Optical image of microarray. The inset is the SEM image of microarray showing the nine individually addressable microelectrodes of 200 μm diameters. (b) Overlay of the cyclic voltammograms of the 10 μm (green), 50 μm (brown) and 100 μm (blue) microarrays. The electrolyte is 5 mM $Fe(CN)_6^{3-/4-}$ in 1 M KCl. (c) Square wave voltammograms of 10 ppm lead on a 100 μm microelectrode after five different deposition times of 0, 5, 25, 55 and 110 s (black to blue curves) at −1.52 V vs. Pt reference/counter. (d) Nyquist plot (dotted curve-experimental and solid curve-fitted) of 200 μm microelectrodes modified with anti-K12 bacteria antibody and casein blocker (blue solid circles) and after K12 bacteria capture (pink solid circles). The optical (inset) images of a clean and *E. coli* K12 captured microelectrodes. The electrolyte used is 5 mM $Fe(CN)_6^{3-/4-}$ in 0.01 M PBS buffer. (e) UNCD coated pre-sharpened tungsten microwire microsensor. The microelectrode is exposed at the tip by insulating with a 3 μm thick parylene and laser etched. (A color version of this figure can be viewed online.)**

sensitive to the surface termination (—H vs. —O), allowing further optimization of electronic properties of these electrodes [55]. The diamond surface termination can be readily modified by chemical treatment in hot concentrated $H_2SO_4$ for an O-terminated surface and with $H_2$ plasma treatment for a fully H-terminated surface. Diamond microelectrode arrays (MEAs, Fig. 9a) are gaining attention for biological and chemical sensing because of their high sensitivity and selectivity, multiplexing capability and low cost [56–59]. Electrochemical characterization studies of BD-UNCD demonstrated minimal variation in current peak separation in cyclic voltammograms from the array (<5%), demonstrating highly uniform, reliable microelectrodes with excellent electrochemical behavior: a quasi-reversible electrode process (the separation between oxidation and reduction peaks, $\Delta Ep \sim 110$ mV) (Fig. 9b); two-Q (Constant Phase Element, CPE) behavior; high S/N ratios of greater than 300 and minimal surface oxidation. The MEAs were successfully employed to detect a wide range of analytes including bacteria [59], dopamine [60], hormones and heavy metals (Fig. 9c–d). BD-UNCD microsensors in microwire geometry (Fig. 9e) are more suitable for *in vivo* voltammetry measurement of neuro active substances. These microwire sensors have been tested by using flow injection analysis and in rat brains for dopamine detection. Detection limits down to 27 nM were achieved. It is notable that due to the unique properties of the UNCD interface such as its chemical stability, ultra-smooth surface morphology and minimal non-specific binding, this new electrochemically robust material could emerge as the next best electrochemical transducer for advanced sensing, particularly in implant applications.

## 5. Conclusions

We have demonstrated boron doped UNCD fabricated with an H-rich/Ar-lean and a high $CH_4/H_2$ ratio gas chemistry in a HFCVD reactor. The BD-UNCD fabrication technique is different from both H-rich but low $CH_4/H_2$ ratio gas chemistry used in conventional NCD/MCD fabrication, and Ar-rich and low $CH_4$/Ar ratio gas chemistry used in the conventional UNCD fabrication in PECVD deposition systems. Low resistivity down to 0.01 ohm cm as measured by 4-point probe, a uniform and small grain size of 5–15 nm as measured by SEM/TEM, a low roughness down to several nm as measured by AFM, and a high purity $sp^3$ content confirmed by NEXAFS, demonstrate that the diamond reported here is a heavily boron doped UNCD with high purity. These measurements also revealed featured

roughness, nano-texture, grain information, and the surface chemistry of BD-UNCD. The results indicate that high purity UNCD is not necessarily linked to low $CH_4$ content and/or Ar-rich gas, and for the first time BD-UNCD has been fabricated in a HFCVD tool mixed with a boron/methane ratio up to 12,500 ppm. Applications of this type of BD-UNCD on conductive AFM probes, robust electrodes and high performance/biocompatible sensors have been demonstrated. An overall hypothesis for the deposition of BD-UNCD in both HFCVD Ar-lean and PECVD Ar-rich conditions arises from the results presented, i.e., that a high renucleation rate and the minimization of non-diamond carbon build-up tends to lead to the formation of UNCD. However, this hypothesis will require further investigation and quantification in the future work, including study on the correlations of morphology (grain size) vs. pressure and $CH_4/H_2$ ratio, $sp^2$ concentration vs. pressure and $CH_4/H_2$ ratio at different temperature, etc.

## Acknowledgements

The work was partially supported by the Defense Threat Reduction Agency under Grant HDTRA109C0007, the National Science Foundation SBIR under Grant 1058505, the Army Research Office STTR under Grant W911NF-12-0102 and the National Institute of Health under Grant 2R44HL108534-02. R.W.C. acknowledges support from the National Science Foundation under Grants DMR-1107642, CMMI-1200019, and support from AFOSR under Contract No. FA2386-11-1-4105 AOARD. F.M. acknowledges support from the Marie Curie International Outgoing Fellowship for 161605-4 Career Development within the 7th European Community Framework Program under Contract No. PIOF-GA-2012-328776. AFM and SEM were conducted by facilities at the Center for Nanoscale Materials (CNM) at Argonne National Lab. Use of the CNM was supported by the U. S. Department of Energy, Office of Science, Office of Basic Energy Sciences, under Contract No. DE-AC02-06CH11357. Use of the Nanocharacterization Facility at the University of Pennsylvania is also acknowledged. The authors thank Grace Catausan, Keith Gantz, Charles West, Sabitha Jose and Matthew Hart for diamond synthesis and data collection, and thank Leonidas Ocola and Ralu Divan at CNM for their help on AFM and SEM imaging.

## REFERENCES

[1] Gruen DM, Liu S, Krauss AR, Luo J, Pan X. Fullerenes as precursors for diamond film growth without hydrogen or oxygen additions. Appl Phys Lett 1994;64:1502–4.
[2] Jiao S, Sumant A, Kirk MA, Gruen DM, Krauss AR, Auciello O. Microstructure of ultrananocrystalline diamond films grown by microwave Ar–$CH_4$ plasma chemical vapor deposition with or without added $H_2$. J Appl Phys 2001;90:118–22.
[3] Krauss AR, Auciello O, Ding MQ, Gruen DM, Huang Y, Zhironv VV, et al. Electron field emission for ultrananocrystalline diamond films. J Appl Phys 2001;89:2958–67.
[4] Gruen DM. Nanocrystalline diamond films. Annu Rev Mater Sci 1999;29:211–59.
[5] Auciello O. Are diamonds a MEMS' best friend? IEEE Microwave Magazine, December, 61–75.
[6] Gruen DM, Liu S, Krauss AR, Pan X. Buckyball microwave plasmas: fragmentation and diamond-film growth. J Appl Phys 1994;75:1758–63.
[7] Philip J, Hessa P, Feygelson T, Butler JE, Chattopadhyay S, Chen KH, et al. Elastic, mechanical, and thermal properties of nanocrystalline diamond films. J Appl Phys 2003;93:2164–71.
[8] Ashfold MNR, May PW, Rego CA, Everitt NM. Thin film diamond by chemical vapour deposition methods. Chem Soc Rev 1994;23:21–30.
[9] Chen Q, Gruen DM, Krauss AR, Corrigan TD, Witek M, Swain GM. J Electrochem Soc 2001;148:E44–51.
[10] Hagans PL, Natishan PM, Stoner BR, O'Gradya WE. Electrochemical oxidation of phenol using boron-doped diamond electrodes. J Electrochem Soc 2001;148:E298–301.
[11] Swain GM, Ramesham R. The electrochemical activity of boron-doped polycrystalline diamond thin film electrodes. Anal Chem 1993;65:345–51.
[12] Rodrigo MA, Michaud PA, Duo I, Panizza M, Cerisola G, Comninellis Ch. Electrode for wastewater treatment oxidation of 4-chlorophenol at boron-doped diamond. J Electrochem Soc 2001;148:D60–4.
[13] Angela A, Urtiaga A, Ortiz I. Pilot scale performance of the electro-oxidation of landfill leachate at boron-doped diamond anodes. Environ Sci Technol 2009;43:2035–40.
[14] Rao TN, Fujishima A. Recent advances in electrochemistry of diamond. Diam Relat Mater 2000;9:384–9.
[15] Carlisle JA. Diamond films precious biosensors. Science 2004;3:668–9.
[16] Majid E, Male KB, Luong JHT. Boron doped diamond biosensor for detection of *Escherichia coli*. J Agric Food Chem 2008;56:7691–5.
[17] Okano K, Naruki H, Akiba Y, Kurosu T, Lida M, Hirose Y. Synthesis of diamond thin films having semiconductive properties. Jpn J Appl Phys 1988;27:L173–5.
[18] Bhushan B, Subramaniam VV, Malshe A, Gupta BK, Ruan J. Tribological properties of polished diamond films. J Appl Phys 1993;74:4174–80.
[19] Konicek AR, Grierson DS, Gilbert PUPA, Sawyer WG, Sumant AV, Carpick RW. Origin of ultralow friction and wear in ultrananocrystalline. Diamond 2008;100. 235502-1–4.
[20] Sumant A, Grierson DS, Gerbi JE, Birrell J, Lanke UD, Auciello O, et al. Toward the ultimate tribological interface: surface chemistry and nanotribology of ultrananocrystalline diamond. Adv Mater 2005;17:1039–45.
[21] Tang L, Tsai C, Gerberich WW, Kruckeberg L, Kania DR. Biocompatibility of chemical-vapour-deposited diamond. Biomaterials 1995;16:483–8.
[22] Zeng H, Arumugam PU, Carlisle JA. Fibrinogen adsorption study on ultrananocrystalline diamond as a biocompatible antithrombogenic interfacial material for implantable devices. Phys Status Solidi A 2014. 201431396-1–4.
[23] Bhattacharyya S, Auciello O, Birrell J, Carlisle JA, Crutiss LA, Goyette AN, et al. Synthesis and characterization of highly-conducting nitrogen-doped ultrananocrystalline diamond films. Appl Phys Lett 2001;79:1441–3.
[24] Birrell J, Carlisle JA, Auciello O, Gruen DM, Gibson JM. Morphology and electronic structure in nitrogen-doped ultrananocrystalline diamond. Appl Phys Lett 2002;81:2235–7.
[25] Show Y, Witek MA, Sonthalia P, Swain GM. Characterization and electrochemical responsiveness of boron-doped nanocrystalline diamond thin-film electrodes. Chem Mater 2003;15:879–88.
[26] Privorotskaya NL, Zeng H, Carlisle JA, Bashir R, King WP. Piezoresistive microcantilevers from ultrananocrystalline diamond. JMEMS 2010;19:1234–42.
[27] Butler JE, Sumant AV. The CVD of nanodiamond materials. Chem Vap Deposition 2008;14:145–60.

[28] Carlisle JA, West CF, Zimmer JW. Diamond film deposition. US Patent Application Publication US 2009/0017258 A1; 2009.
[29] Liu H, Dandy DS. Studies on nucleation process in diamond CVD: an overview of recent developments. Diam Relat Mater 1995;4:1173–88.
[30] Moldovan N, Dai Z, Zeng H, Carlisle JA, Jacobs TDB, Vahdat V, et al. Advances in manufacturing of molded tips for scanning probe microscopy. JMEMS 2012;21:431–45.
[31] Sumant AV, Gilbert PUPA, Griesron DS, Konicek AR, Abrecht M, Butler JE, et al. Surface composition, bonding, and morphology in the nucleation and growth of ultra-thin, high quality nanocrystalline diamond films. Diam Relat Mater 2007;16:718–24.
[32] Gajewski W, Achatz P, Williams OA, Haenen K, Bustarret E, Stutzmann M, et al. Electronic and optical properties of boron-doped nanocrystalline diamond films. Phys Rev B 2009;79. 045206-1–14.
[33] Bhattacharyya S. Mechanism of high n-type conduction in nitrogen-doped nanocrystalline diamond. Phys Rev B 2004;70:125412.
[34] Zeng H, Arumugam PU, Siddiqui S, Carlisle JA. Low temperature boron doped diamond. Appl Phys Lett 2013;102. 223108-1–5.
[35] Birrell J, Gerbi JE, Auciello O, Gibson JM, Johnson J, Carlisle JA. Interpretation of the Raman spectra of ultrananocrystalline diamond. Diam Relat Mater 2005;14:86–92.
[36] Zaitsev AM. Optical Properties of Diamond – A Hand Book. Berlin Heidelberg New York: Springer-Verlag; 2003. 89–102.
[37] Prawer S, Nugent KW, Jamieson DN, Orwa JO, Bursill LA, Peng JL. The Raman spectrum of nanocrystalline diamond. Chem Phys Lett 2000;332:93–7.
[38] Ferrari AC, Robertson J. Origin of the 1150-$cm^{-1}$ Raman mode in nanocrystalline diamond. Phys Rev B 2001;63. 121405-1–4.
[39] Zhang RJ, Lee ST, Lam YW. Characterization of heavily boron-doped diamond films. Diam Relat Mater 1996;5:1288.
[40] Ushizawa K, Watanabe K, Ando T, Sakaguchi I, Nishitani-Gamo M, Sato Y, et al. Boron concentration dependence of Raman spectra on 100 and 111 facets of B-doped CVD diamond. Diam Relat Mater 1998;7:1719–22.
[41] Pruvost F, Bustarret E, Deneuville A. Characteristics of homoepitaxial heavily boron-doped diamond films from their Raman spectra. Diam Relat Mater 2000;9:295–9.
[42] Sumant AV, Grierson DS, Gerbi JE, Carlisle JA, Auciello O, Carpick RW. Surface chemistry and bonding configuration of ultrananocrystalline diamond surfaces and their effects on nanotribological properties. Phys Rev B 2007;76. 235429-1–11.
[43] Stohr J. NEXAFS Spectroscopy. Berlin, Heidelberg: Springer-Verlag; 1992. 162–210.
[44] Williams OA, Daenen M, D'Haen J, Haenen K, Maes J, Moshchalkov VV, et al. Comparison of the growth and properties of ultrananocrystalline diamond and nanocrystalline diamond. Diam Relat Mater 2006;15:654–8.
[45] Sharda T, Umenoc M, Soga T, Jimbob T. Growth of nanocrystalline diamond films by biased enhanced microwave plasma chemical vapor deposition. Diam Relat Mater 2001;10:1592–6.
[46] Sowers AT, Ward BL, English SL, Nemanicha RJ. Field emission properties of nitrogen-doped diamond films. J Appl Phys 1999;86:3973–82.
[47] Lifshitz Y, Lee CH, Wu Y, Zhang WJ, Bello I, Lee ST. Role of nucleation in nanodiamond film growth. Appl Phys Lett 2006;88. 243114-1–3.
[48] Agrawal R, Moldovan N, Espinosa HD. An energy-based, model to predict wear in nanocrystalline diamond atomic force microscopy tips. J Appl Phys 2009;106. 064311-1–6.
[49] Liu J, Notbohm JK, Carpick RW, Turner KT. Method for characterizing nanoscale wear of atomic force microscope tips. ACS Nano 2010;4:3763–72.
[50] Tsukruk VV, Singamaneni S. Scanning Probe Microscopy of Soft Matter: Fundamentals and Practices. Wiley-VCH; 2012. pp. 52.
[51] Su C, Huang L, Kjoller K, Babcock K. Studies of tip wear processes in tapping mode atomic force microscopy. Ultramicroscopy 2003;97:135–44.
[52] Fletcher PC, Felts JR, Dai Z, Jacobs TD, Zeng H, Lee W, et al. Wear-resistant diamond nanoprobe tips with integrated silicon heater for tip-based nanomanufacturing. ACS Nano 2010;4:3338–44.
[53] Chaplin BP, Wyle I, Zeng H, Carlisle JA, Farrell J. Characterization of the performance and failure mechanisms of boron-doped ultrananocrystalline diamond electrodes. J Appl Electrochem 2011;41:1329–40.
[54] McCreery RL. Advanced carbon electrode materials for molecular electrochemistry. Chem Rev 2008;108:2646–87.
[55] Nebel CE, Shin D, Rezek B, Tokuda N, Uetsuka H, Watanabe H. Diamond and biology. J R Soc Interface 2007;4:439–61.
[56] Cvacka J, Quaiserova V, Park J, Show Y, Muck A, Swain GM. Boron-doped diamond microelectrodes for use in capillary electrophoresis with electrochemical detection. Anal Chem 2003;75:2678–87.
[57] Simm AO, Banks CE, Ward-Jones S, Davies TJ, Lawrence NS, Jones TG, et al. Boron-doped diamond microdisc arrays: electrochemical characterisation and their use as a substrate for the production of microelectrode arrays of diverse metals (Ag, Au, Cu) via electrodeposition. Analyst 2005;130:1303–11.
[58] Hu J, Holt KB, Foord JS. Focused ion beam fabrication of boron-doped diamond ultramicroelectrodes. Anal Chem 2009;81:5663–70.
[59] Siddiqui S, Dai Z, Stavis CJ, Zeng H, Moldovana N, Hamers RJ, et al. A quantitative study of detection mechanism of a label-free impedance biosensor using ultrananocrystalline diamond microelectrode array. Biosens Bioelectron 2012;35:284–90.
[60] Arumugam PU, Zeng H, Siddiqui S, Covey DP, Carlisle JA, Garris PA. Characterization of ultrananocrystalline diamond microsensors for in vivo dopamine detection. Appl Phys Lett 2013;102. 253107-1–5.